www.czasopisma.pan.pl PAN POLSKA AKADEMIA NAUK www.journals.pan.pl

Arch. Metall. Mater. **68** (2023), 4, 1503-1512

DOI: https://doi.org/10.24425/amm.2023.146216

A. NALBORCZYK-KAZANECKA[1,2*], G. MRÓWKA-NOWOTNIK[1], A. PYTEL[1,2]

THE EFFECT OF THE HEAT TREATMENT CONDITION OF THE BASE MATERIAL ON THE MICROSTRUCTURE AND MECHANICAL PROPERTIES OF 17-4PH STAINLESS STEEL ELECTRON BEAM WELDED JOINTS

The study was intended to determine the effect of the input condition of the 17-4PH steel on the microstructure, mechanical properties and stress state of welded joints. The steel adopted for testing was in the solution condition at 1040°C, the aged condition at 550°C/4h and the overaged condition at 760°C/2 h + 620°C/4 h. Samples of 17-4PH steel, after heat treatment processed with different parameters, were electron beam welded (EBW). The microscopic observation (LM, SEM/EDS) showed that the microstructure of the weld consisted of martensite with a δ-ferrite lattice. In the heat-affected zone (HAZ), transformed martensite was found with evidence of niobium carbides. The results of hardness testing revealed the different nature of the hardness profile with the condition the material before the EB welding process. The hardness profile of the HAZ of the welded samples in the as-solution (ES2) and overaged (ES12) condition was varied (from about 340 HV to 450 HV). However, in the aged condition specimen of 17-4PH steel (ES22) showed a similar hardness level, at around 370 HV. The solution condition (ES2) had the highest strength properties R_m 1180.6 MPa with the lowest elongation A 7.6% of all samples tested. The aged welded specimen (ES22) retained high strength R_m 1103.4 MPa with a better relative elongation A 10.1%, whereas the overaged welded specimen (ES12) saw a reduction of strength R_m 950.4 MPa with an improvement in plastic properties A 18.8%. Obtained results showed a significant effect of the input steel condition on the obtained EB welded joints.

Keywords: welding; 17-4PH; heat treatment; EB welding

1. Introduction

17-4PH steel belongs to the group of precipitation heat treated martensitic steels. It is an important structural material used in the aerospace or nuclear industries due to its high strength properties with the preservation of good corrosion resistance. Such steels are heat treated in order to obtain the desired mechanical properties. The heat treatment consists of the following processes: solutioning and ageing. During solutioning, in addition to the dissolution of alloying elements in the matrix, a martensitic transformation occurs. These steel are characterised by a low carbon martensitic matrix, the so-called soft martensite. Apart from martensite, they may also contain ferrite, as well as residual austenite [1]. In case of 17-4PH precipitation-hardened martensitic steel, the solution heat treatment is conducted at 1040°C, while the holding time is 0.5 to 1 hour [1-3]. The Ac_1 and Ac_3 temperatures are approximately 627°C and 704°C, respectively [4,5]. The solution heat treatment carried out at a lower temperature causes lower strength properties due to lower dissolution of carbon and copper in austenite. The overheated solution heat treatment also reduces the strength properties as a result of austenite retention in the matrix, as well as it causes austenite grain growth [1-3,6]. The solubility rate of copper at 1040°C is approximately 7%, while the copper content in grade 17-4PH steel is 3-5% wt., which allows the matrix to be dissolved and saturated with copper elements during the solutioning process [1-3].

In the solution heat treatment, austenite transforms into martensite during cooling. The martensitic transformation start temperature, M_s, is 130°C, while the end temperature of the process, M_f, is 30°C [1]. The solution results in low-carbon lath martensite (BCC) saturated with alloying elements. This martensite has high dislocation density [7,8]. During ageing, high-copper hardening precipitates known as CRPs (Cu-rich precipitates) are formed [9,13]. Matrix-coherent precipitates with a BCC structure are transformed into partially coherent precipitates with a 9R structure. BCC-structured and 9R-structured CRPs can reach diameters of several nm [3,7,10-12]. The continuation of the age-

[1] RZESZÓW UNIVERSITY OF TECHNOLOGY, FACULTY OF MECHANICAL ENGINEERING AND AERONAUTICS, 12 POWSTAŃCÓW WARSZAWY AV., 35-959 RZESZÓW, POLAND
[2] PRATT & WHITNEY RZESZÓW, RZESZÓW, POLAND

* Corresponding author: agnieszka.nalborczyk@prattwhitney.com

ing process leads to a complete loss of particle-to-matrix coherence and the transformation of the particles into FCC-structured precipitates. The flowchart of Cu-rich particle precipitation is as follows: BCC → 9R → FCC [3,7,11]. The ageing of 17-4PH steel is carried out within the temperature range of 480-620°C [1].

17-4PH steel is characterised by weldability in the solution condition (1040±15°C) or in the overaged condition (1040±15°C + 760°C/2 h + 620°C/4 h). In contrast, welding of the steel on the aged condition (1040±15°C + 480°C/1 h) is not recommended [1]. The previous studies focused on the influence of the post welding heat treatment (PWHT) on microstructure and mechanical properties [14,15]. Also, focused on identifying the causes of weld defects such as microcracking, solidification cracking or porosity [16,17]. Researches did not focus on the impact of pre-heat treatment on welded joints.

My earlier study [18] was focused on the effect of welding parameters (GTAW method) on the microstructure of a welded joint in a solution condition. The research study showed the influence of the welding process on the microstructure of the heat-affected zone 17-4PH stainless steel. In order to determine the effect of the heat treatment condition of the base material on the microstructure and mechanical properties of welded joints, the research was continued.

Welding is a widely used process for joining aircraft engine components. The best quality of welded joints is required. Hance, GTAW or EBW methods are used in aerospace industry. One of the most important advantages of electron beam welding is ability to create single-pass, narrow and deep-penetrated weld with a heat input that is much lower than in arc welding method. The lower heat input results in a narrow heat affected zone (HAZ) and reduces the effect of heat on the welded material. Electron beam welding gives the ability to weld materials thicknesses of less than 0.5 mm up to 300 mm. Vacuum provides protection against oxidation. These are just some of the many advantages, but they contribute to the quality of the welded joints is high. Accordingly, this method was used in this study [19,20].

This research paper focuses on determining the effect of steel heat treatment prior to the welding process on the microstructure, mechanical properties and stress condition of welded joints.

2. Methodology

The welding process was performed using a high-energy welding method, namely electron beam welding (EBW), on 1.6 mm thick, flat samples prepared made of 17-4PH steel (AMS5604) (Fig. 1). The steel sheet was provided in the solution condition (1040±15°C). The samples taken for testing measured 5×127 mm. The joints were welded on the samples representing three heat treatment conditions (TABLE 1).

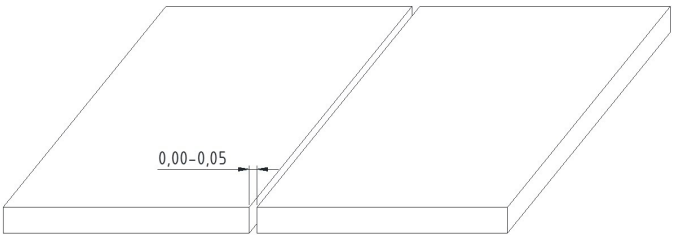

Fig. 1. The weld joint configuration

The surfaces of the samples were mechanical cleaned before welding, then they were cleaned with isopropyl alcohol. The welded joints were made using STEIGERWALD STRAHLTECHNIK KS54-G150KM EB welding machine. Before the actual welding process, 2 tack-weld points were made at the ends of the steel sheets to avoid the formation of gaps during the welding process. For the test samples in different conditions of heat treatment, butt welded joints were made with the welding parameters shown in TABLE 2. The samples were welded using a circular oscillation pattern, in 10^{-4} Torr vacuum atmosphere.

TABLE 1

The sample designations and heat treatment condition

Sample designation	Sheet metal delivery condition	Pre-welding heat treatment
ES2 Sample	Solution, 1040°C/1h	—
ES12 Sample		Overaging 760°C/2h+ 620°C/4h
ES22 Sample		Solution 1040°C/1h + aging 550°C/4h

The residual stresses within the welded joint area were determined using a Proto Manufacturing's iXRD diffractometer. The sin2ψ method and the XRD Win 2.0 computer software were used to calculate the stress values. A CuKα X-ray beam with a wavelength of λ = 0.154 nm and a diameter of 1 mm, anode voltage of 20 kV and anode current of 4 mA was used. The residual stress was determined for seven different values of ψ angle ranging from –30° to 30°. For each test sample, measurements were taken in two areas, at 3 different points – one in the weld area and two in the HAZ (Pt1-Pt3, see Fig. 2).

The microstructure of the welded joints was studied on the cross sections using a Leica DMI 3000M light microscope

TABLE 2

The welding parameters

Sample number	Operations	U [kV]	I [mA]	FOC [mA]	v [mm/s]	Deviation			
						x [mm]	y [mm]	Hz	b
ES2 ES12 ES22	Tack-welding	120	5	–10	20	0.6	0.6	800	circular
	Welding	120	14.5	–40	20	0.9	0.9	800	circular

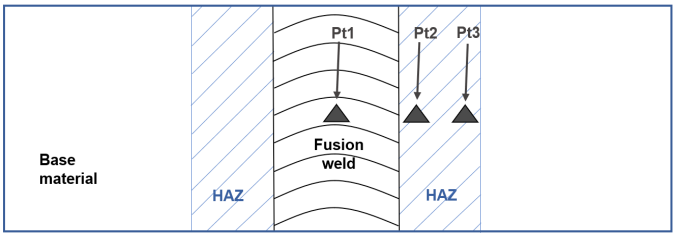

Fig. 2. The locations of stress measurement points on the weld joints

and a Hitachi S-3400N scanning electron microscope with EDS X-ray microanalysis. The metallographic specimens were prepared by standard methods using Struers machines. The observation was carried out in the Kallings reagent etched condition.

The hardness was measured within the welded joint area on the cross-sections. The Vickers method was applied at a load of 500 g (5 N), (10 s dwell time) using an Innovatest Nexus 4303 microhardness tester. A series of measurements was taken on each specimen including the base metal and the weld (Fig. 3).

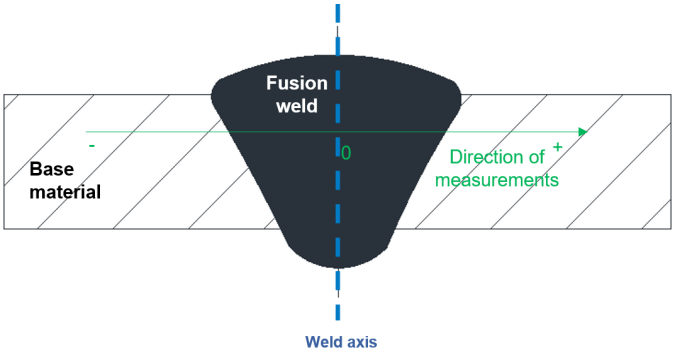

Fig. 3. The area and orientation of HV hardness measurements

A static tensile test was performed to determine the mechanical properties. Flat samples with standard dimensions were used (Fig. 4). The tests were carried out using an INSTRON 8801 universal testing machine acc. to PN-EN ISO 6892 1:2016. $Rp_{0.2}$ yield strength, R_m tensile strength and A_5 elongation were determined.

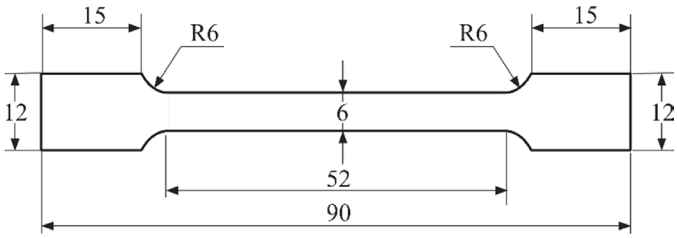

Fig. 4. The shape and dimensions of samples for the static tensile test

3. Results and discussion

3.1. Microstructure

Based on the observation of the microstructure, it was found out that the welds were characterised by a columnar dendritic microstructure. For all the welds, an increase in grain size in the direction of the weld centreline was observed (Fig. 5a,c,e). The crystallites met within the weld centreline, forming a characteristic line. This microstructure favours the formation of crystallisation cracks, but the applied welding parameters allowed to avoid this type of defects. The weld consists of martensite with a δ-ferrite lattice at the boundaries of the prior austenite grain. In addition, microstructure studies revealed a discontinuity in welded joint

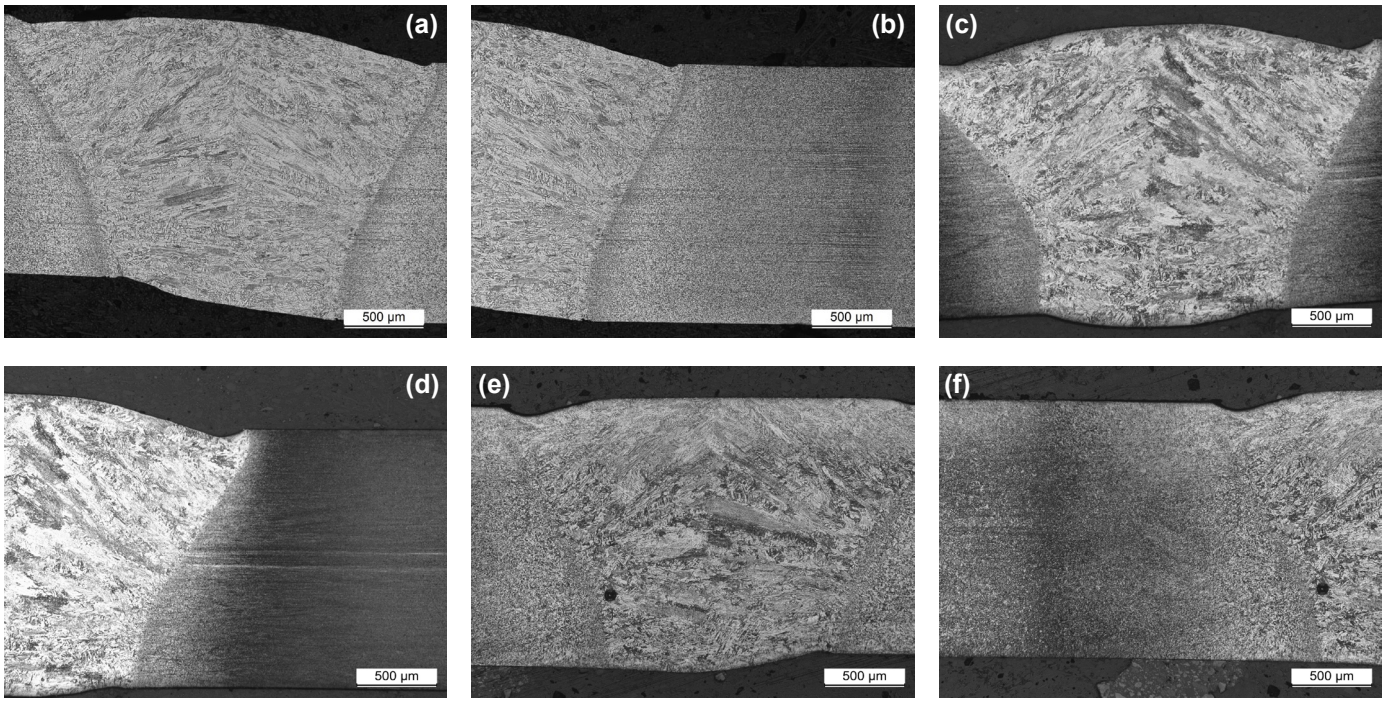

Fig. 5. The welded joint microstructure: (a),(b) ES2 sample – welded in the solution condition; (c),(d) ES12 sample – welded in the 720°C/2 h + 620°C/4 h aged condition; (e),(f) ES22 sample – welded in the 550°C/4h aged condition

ES22 that was a pore, located at the fusion boundary. No such discontinuities were found in welded joints of ES2 and ES12.

The appearance of the HAZ varies considerably depending on the heat treatment condition of the parent material. During welding, the heat released interacts with the base metal, leading to a change of the microstructure. In the HAZ of ES2, ES12 and ES22 samples, δ-ferrite was found at the fusion boundary, which results from the fact that the material in the vicinity of the weld is heated to the temperature of δ-ferrite, A_{c5}. As a result of rapid cooling, the diffusive transformation of ferrite into austenite is stopped. The δ-ferrite lattice is present at the martensite grain boundaries. δ-ferrite bands oriented in the sheet rolling direction can also be seen in the HAZ. The literature data suggest [1] that the quantity of δ-ferrite in 17-4PH steel can reach up to 10%. For all the samples, grain growth was observed in the HAZ at the weld.

On the ES2 weld (Fig. 6b), coarse-grained martensite (A) gradually changes into fine-grained martensite (B). The coarse-grained martensite area and the fine-grained martensite area consist of newly formed martensite (the welding process

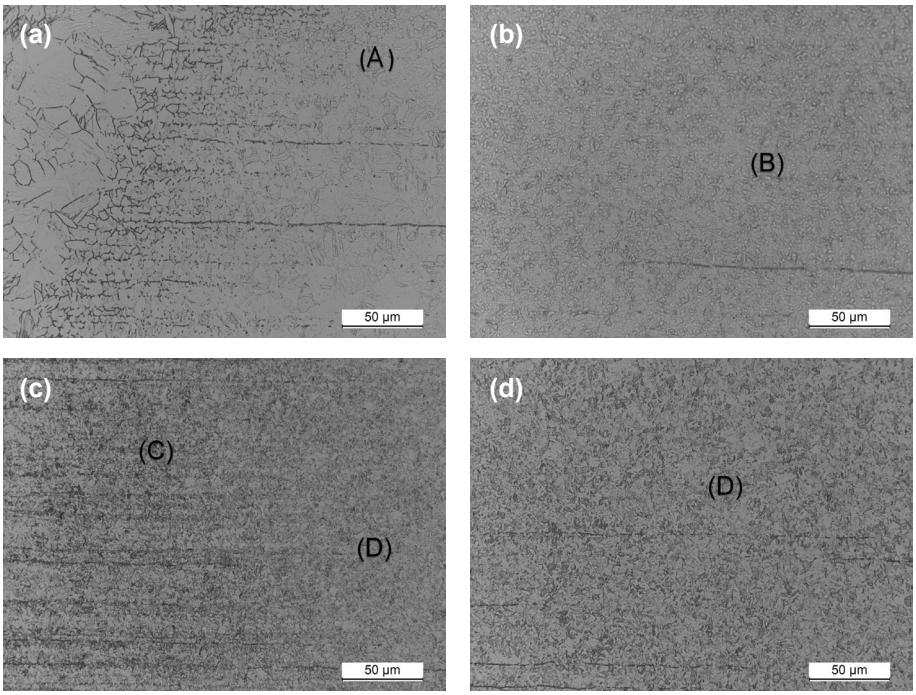

Fig. 6. The microstructure of the welded joint – ES2 sample: (a) fusion boundary with noticeable δ-ferrite; (b) fine-grained martensite; (c) dark-grained area; (d) transition of the HAZ into the base metal

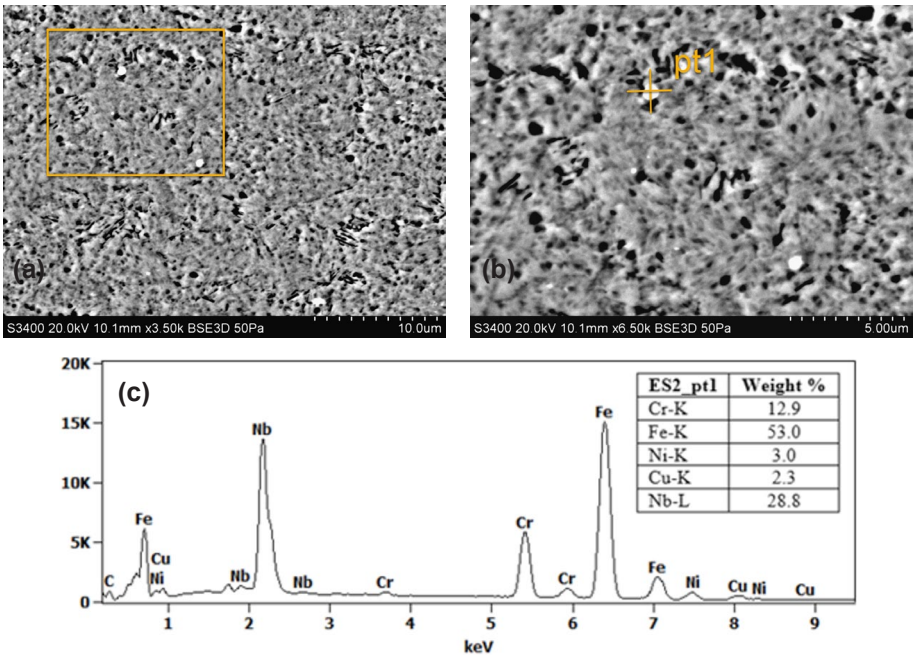

Fig. 7. The microstructure of the welded joint: ES2 sample and scattered X-ray energy spectrum in EDS analysis

causes an increase in the temperature in this area above Ac_3, and during cooling there occurs a non-diffusive transformation of austenite into martensite). Then the fine-grained microstructure (B) turns into a dark-etched area (C) (Fig. 6c). The presence of NbC carbides was observed in the dark etched area (Fig. 7). The temperature of exposure in the area (C) was lower than in the zone adjacent to the weld, so no carbide dissolution occurred. Based on the literature data and the observation of the microstructure, it can be assumed that this area was exposed to the temperatures between Ac_1 and Ac_3. A part of martensite was therefore transformed into austenite during heating at the time of the welding process. The area (D) further out was exposed to a temperature lower than Ac_1. The observation of the microstructure by SEM and light microscopy did not reveal any changes in the base metal (Fig. 6d).

In the HAZ of the ES12 sample welded in the overaged condition, it is possible to distinguish a brightly etched area (E), right at the weld (Fig. 8a). In this area, there is a transfor-

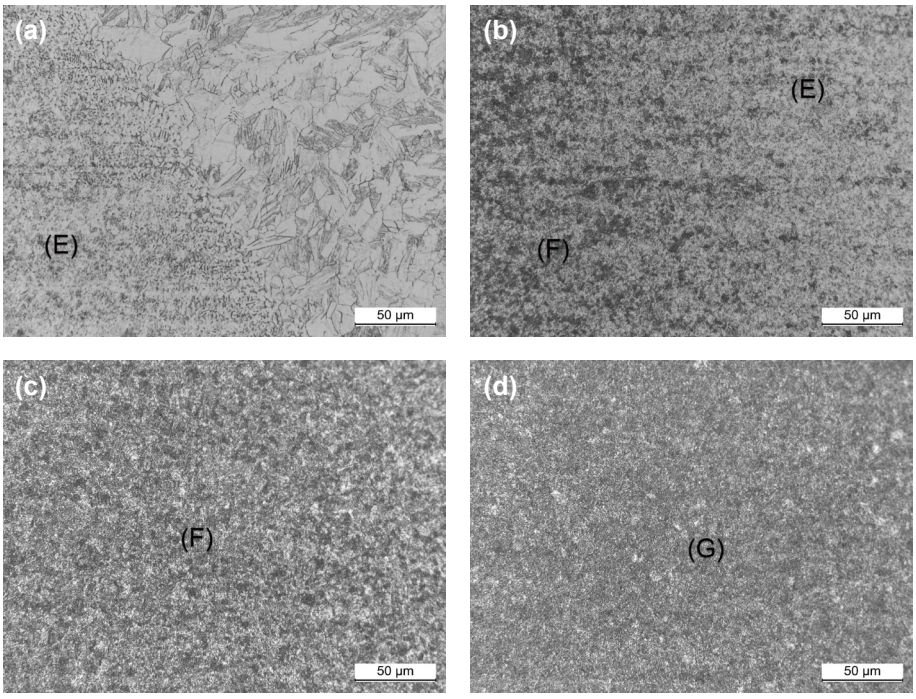

Fig. 8. The microstructure of the welded joint, ES12 sample: (a) fusion boundary with visible δ-ferrite; (b) fine-grained martensite turning into the dark etched area; (c) dark etched area; (d) base metal

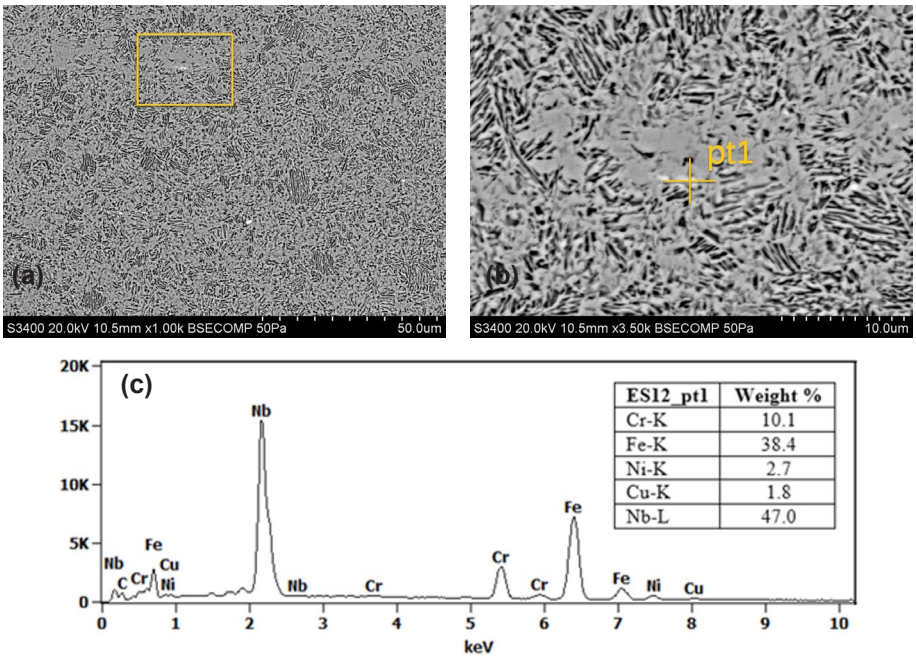

Fig. 9. ES12 sample – the welded joint microstructure and results of chemical composition analysis (EDS): scattered X-ray energy spectrum and content levels of chemical elements

mation of highly overaged martensite under the influence of heat, resulting in 'fresh' martensite (Fig. 8a). As the distance from the weld increases, this area turns into the dark etched zone (F), where an area of the coexistence of the newly formed and overaged martensite can be seen (Fig. 8b). This area was exposed to temperatures ranging from Ac_1 to Ac_3. During the observation of the dark-etched area, the presence of NbC was observed (Fig. 9). The base metal (G) is also characterised by a dark etched area where highly overaged martensite is present (Fig. 8d). In this martensite, CRPs were formed during the heat treatment. Due to a small size of CRPs they were not observed during the SEM examination.

The HAZ of the ES22 welded joint at the weld also consists of newly formed and transformed martensite (H), where grain growth can be visually observed (Fig. 10a). As the distance from the weld increases, the grain size (I) decreases (Fig. 10b). The area (I) turns into the area with darker etching (J), similarly as in the case of ES2 welded joints, suggesting that this area was

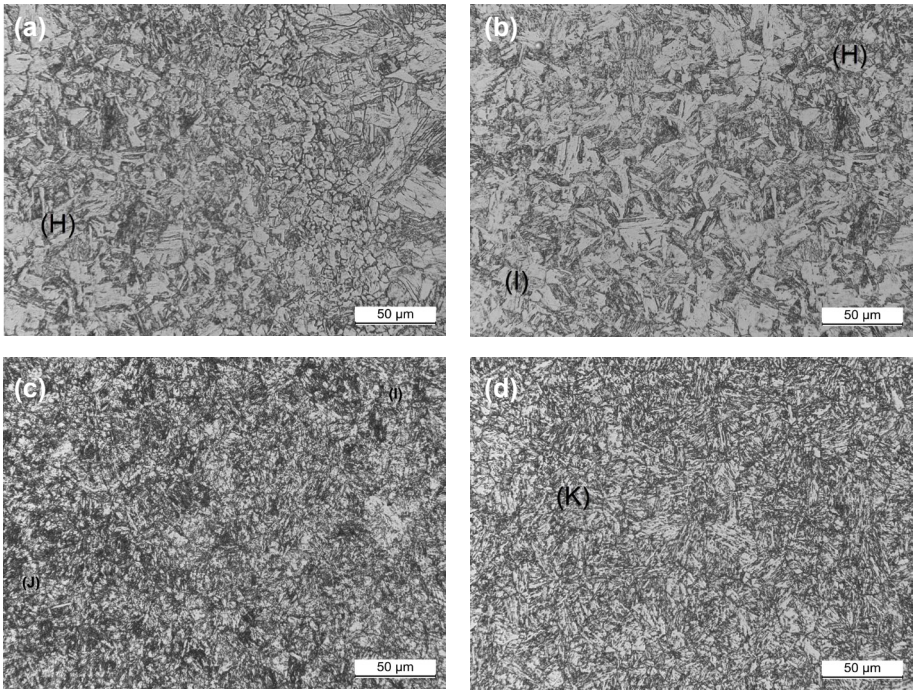

Fig. 10. ES22 sample – the welded joint microstructure: (a) fusion boundary with visible δ-ferrite; (b) martensite (c); dark etched area; (d) base material

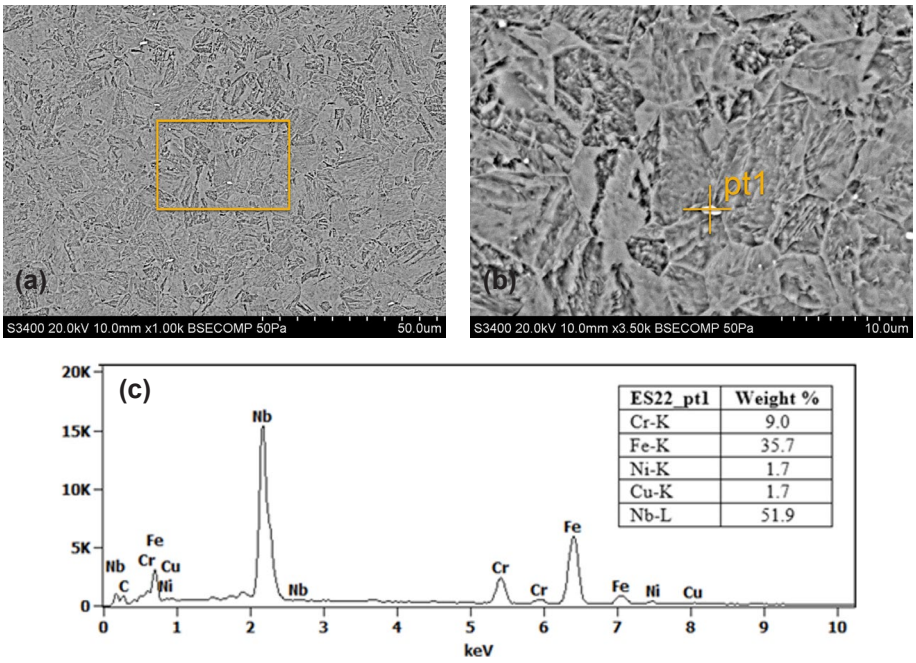

Fig. 11. ES22 sample – the welded joint microstructure and results of chemical composition analysis (EDS): scattered X-ray energy spectrum and content levels of chemical elements

also heated up to the temperature range of Ac_1-Ac_3 (Fig. 10c). NbC can be seen in the microstructure (Fig. 11). Further on, the HAZ transitioned into the base metal, i.e. the aged martensite (K) (Fig. 10d).

3.2. Mechanical properties

In order to determine the mechanical properties, the hardness of the welded joints was measured. The hardness levels within the weld areas of the welded samples in different heat treatment conditions are similar, amounting to respectively: ES2 350-366 HV, ES12 343-369 HV, and ES22 355-373 HV. In contrast, the hardness profile within the HAZ varies significantly among the particular samples (Figs. 12-14).

The ES2 solution welded sample is characterised by the greatest changes of hardness within the area of the welded joint (Fig. 12). The hardness of the weld is by approx. 10 HV lower than that of the base metal. A decrease of hardness was observed at the fusion boundary, which may be related to the grain growth. Further on, the hardness begins to increase. The highest hardness value, reaching up to 454 HV, occurs at a distance of approx. 3.5 mm from the weld centreline. Such hardness distribution results from the ageing process triggered by exposure to heat during the welding process. Then the hardness decreases, reaching the hardness value of the base metal. The exposure to the temperature range of 480-620°C triggers the precipitation of copper-rich particles (CRPs). Due to the short exposure time and a temperature below Ac_1, the changes in the microstructure in this area are not visible during the observation by light microscopy. The difference in the hardness between the weld area and the HAZ at the local hardness peak is approx. 90 HV.

Fig. 12. ES2 sample: the hardness profile of the welded joint

For the ES12 (Fig. 13) and ES22 (Fig. 14) welded joints, there is also an apparent decrease in hardness in the HAZ at the fusion boundary, which is also related to the growth of the prior austenite grain. The hardness of the welded joint for ES12 sample is higher than that of the base metal (310 HV). In the HAZ, the hardness begins to decline at a distance of approx. 2 mm from the weld centreline. In the area of the hardness exceeding the base metal hardness, a martensitic transformation took place as a result of the heat effect during cooling and 'fresh' martensite was formed, as confirmed by the observation of the microstructure. The martensite of the base metal has low hardness as a result of the ageing process – the growth of hardening phases and the reduction in dislocation density. In case of ES22 sample, the hardness in the welded joint remains at a similar level. Both the weld and the HAZ after welding are characterised by similar hardness values. The increase in hardness of ES12 and ES22 samples is not distinct as in case of ES2 because the base metal has already been aged and the particles of hardening phases are present in the microstructure. The short time of exposure of the base metal to heat in the aged condition no longer has a significant effect on the precipitation of hardening phases. On the other hand, it had a major impact on the material in the solution condition.

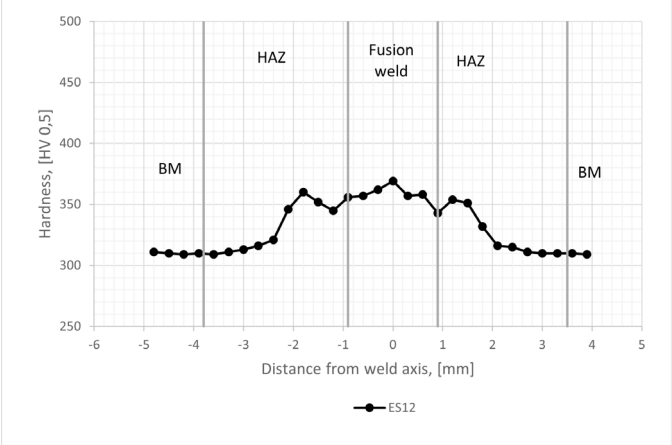

Fig. 13. ES12 sample: the hardness profile of the welded joint

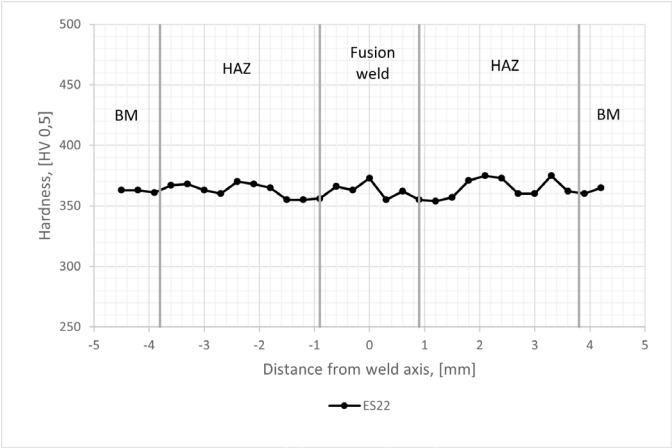

Fig. 14. ES22 sample: the hardness profile of the welded joint

While examining the hardness variation, it's important to consider the microstructure of the welded joints. In the case of the ES2 sample, the grain growth, likely a result of the welding heat, can contribute to the observed decrease in hardness at the fusion boundary. In contrast, the increase in hardness away from the weld centerline may be attributed to a localized age-

ing process, induced by the heat during welding, leading to the precipitation of copper-rich particles.

For the ES12 and ES22 samples, the decrease in hardness in the HAZ at the fusion boundary could also be linked to grain growth from the heat of welding. However, the observed increase in hardness in the weld joint and the subsequent decline in the HAZ might be due to the formation of 'fresh' martensite as a consequence of cooling following the welding process. This transformation could lead to the hardening of the microstructure, thus enhancing the hardness value above that of the base metal.

It's crucial to understand that these hardness variations are a direct consequence of the changes in the microstructure caused by the welding process. The microstructure of the material in the fusion zone, HAZ, and the base metal could be dramatically different, leading to variations in hardness. These microstructural changes should be further examined using microscopy techniques to visualize and quantify the microstructural constituents in order to provide a more comprehensive understanding of the observed hardness variations.

On order to determine the effect of heat treatment on the strength properties of the welded joints, the samples were subjected to static tensile testing after the welding process (four specimens were taken for each parameter). The results (the arithmetic mean of 4 measurements) are shown in TABLE 3. ES2 sample welded in the solution condition is characterised by the lowest elongation of 7.6%, it is characterised by the highest tensile strength of 1180 MPa. ES22 sample also shows a high strength limit of 1103.4 MPa, with the simultaneous increase in elongation to 10.1%. ES12 sample achieved the highest elongation, 18.8%, with the lowest tensile strength of 950.4 MPa. For all the samples, the location of break was in the HAZ. Heat treatment by ageing allows to preserve high strength properties close to the solution condition while improving the ductility of the material. The overaged condition significantly improves the ductility of 17-4PH steel.

TABLE 3

The mechanical properties – tensile strength, yield strength and relative elongation of the ES2, ES12, and ES22 welded joints

Sample designation	$Rp_{0.2}$ [MPa]	R_m [MPa]	Elongation [%]
ES2	893.3	1180.6	7.6
ES12	731.3	950.4	18.8
ES22	917.5	1103.4	10.1

In order to determine the effect of the input condition of the material on the stress state in the welded joint, residual stresses were measured (TABLE 4 and Fig. 15). The state of residual stress in a welded joint is very important for several reasons. Residual stress contributes to the formation of defects in welded joints such as cracking, fatigue strength reduction, stress corrosion cracking. They can also contribute to the formation of cracks, during exploitation which is very important from the safety point of view. The components must meet the requirements – the conditions of dimensions, for the aerospace or nuclear industry the tolerances are very tight. Residual stress may consequently lead to deformation, as a result of that parts will not meet the requirements.

The weld (Pt 1 – Fig. 2) shows positive tensile stresses, the highest of which reaches 319 MPa in the ES2 sample. Notably, these stresses are not uniformly distributed and vary significantly across the weld. This variation in tensile stress across the weld indicates that the cooling rates during welding were not uniform, possibly due to the differences in thermal conductivity in different regions of the weld joint. This heterogeneity is further underlined by the high measurement error value of 319.89±52.46 MPa, which, although relatively high compared to other measurements, may be an indication of the variability in the internal stress states due to the welding process. The weld is characterized by a heterogeneous microstructure with large grain sizes, which could potentially impact the observed stress distribution. As the different grains are exposed to varying degrees of thermal cycles during welding, they could respond differently, leading to variations in stress.

In the Heat-Affected Zone (HAZ) of the welded joint, whose base metal was solution heat-treated, negative (compressive) stresses occur. At the fusion boundary (Pt 2 – Fig. 2), the stress value is –60.65 MPa, while in the HAZ (Pt 3 – Fig. 2) it reaches up to –274.14 MPa. This shift from tensile stresses in the weld to compressive stresses in the HAZ suggests differential cooling rates and thermal contractions in these regions.

For the joints welded in the overaged condition (ES12 sample), the absolute value of compressive stress is slightly higher, –72.98 MPa, while the stress state in the HAZ reaches lower values, –103.43 MPa. This variation in stress values further illustrates the influence of aging heat treatment on the stress distribution, possibly due to changes in the microstructural characteristics of the 17-4PH steel. The aging causes the precipitation of elements, copper in this instance, in the form of hardening phases and a decrease in dislocation density, which contributes to a decrease of residual stresses.

Welding the aged condition (ES22 sample) introduces a slightly different distribution of residual stresses in the weld area (Pt 1 – Fig. 2) and in the HAZ directly adjacent to the weld (Pt 2 – Fig. 2). Tensile stresses occur (approximately 273 MPa and 73 MPa, respectively) in the farther part of the HAZ, transitioning into compressive stresses (approximately –203 MPa) (Pt 3 – Fig. 2).

Such a distribution of stress in the welded joint area is intrinsically linked to the processes occurring during welding due

TABLE 4

The results of residual stress testing in the welded joint areas of 17-4PH steel

Weld joint No.	Residual stress, [MPa]		
	Point 1 – Fusion weld	Point 2 – HAZ	Point 3 – HAZ
ES2	319.89±52.46	–60.65±27.83	–274.14±9.62
ES12	258.14±56.36	–72.98±29.35	–103.43±6.47
ES22	282.61±26.08	72.95±24.96	–202.93±7.36

to temperature exposure. The thermally induced metallurgical transformations, such as the dissolution of alloying elements during the solution treatment and precipitation of copper during aging, significantly influence the resultant stress state, thereby impacting the overall performance of the welded joint.

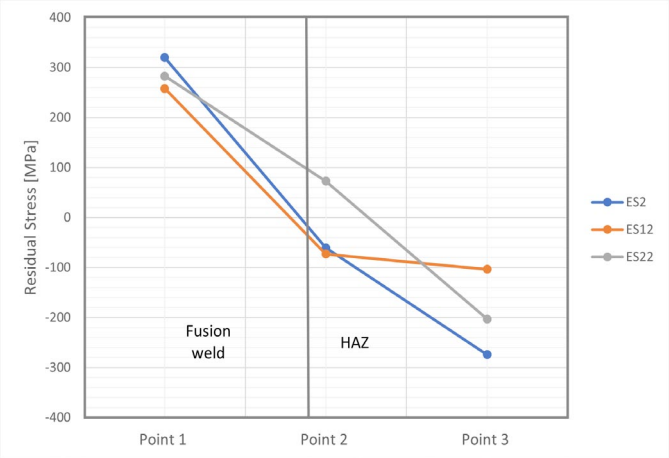

Fig. 15. Residual stresses in the ES2, ES12, and ES22 welded joints

4. Conclusions

The observation of the microstructure reveals changes in the area of the HAZ as a result of exposure to heat. Exposure to temperatures above Ac_3 near the weld causes transformation, as a result of which transformed martensite can be seen. No carbides were noticed in this area. As the distance from the weld increases, the exposure temperature decreases. In the area heated within the Ac_1-Ac_3 range, NbC carbides are present. The nature of transformation for all the samples is the same.

The hardness profile of the HAZ in the sample welded in the solution condition is varied. The hardness increases from approx. 340 HV to 450 HV as a result of a triggered ageing process – the precipitation of hardening CRPs. As the distance from the weld centreline increases, the hardness decreases to approx. 370 HV. The welded joint of sample in the solution condition is characterised by the highest tensile strength of 1080.6 MPa, but the lowest relative elongation, A of 7.6%. In the HAZ, there occur compressive stresses of –60.65±27.83 MPa, whose absolute value increases to –274.14±9.62 MPa. The solution condition is characterised by the highest relative stress values prevailing in the welded joint.

In the overaged condition, the HAZ reaches its highest hardness in the immediate vicinity of the weld, reaching 350 HV, followed by a decrease to 310 HV. The hardness measurements show that the temperature has no significant effect on the hardening phases present in the microstructure. The joint welded in the overaged condition is characterised by lower strength properties, 950.4 MPa, with elongation, A, reaching its highest values of 18.8%. Similarly as in the case of the sample in the overaged condition, the residual stresses in the HAZ become compressive, ranging from –72.98±29.35 MPa to –103.43±6.47 MPa.

The hardness of the welded joints in the aged condition remains at a similar level throughout the joint area, of approx. 370 HV. The aged condition allows to obtain high strength properties of 1103.4 MPa and at the same time it improves the plastic properties, with the relative elongation of 10.1%. In the HAZ at the weld, tensile stresses of 72.95±24.96 MPa are present, which change to compressive stresses of –202.93±7.36 MPa as the distance from the weld increases.

The heat treatment applied to the base material significantly affects the welded joints obtained. The main difference that can be found is the effect of heat on the precipitation hardening process, which starts in the solution condition causing significant differences in in the hardness of the welded joint area. The application of identical welding parameters, with the varied strength test results and the course of the hardness profile, indicates a considerable effect of the base material condition on the properties of the welded joints. It may be assumed that the condition of the input material can generate welding defects, which gives the basis for further research.

REFERENCES

[1] ASM Handbook, Volume 4D: Heat Treating of Irons and Steels ASM International, 2014.

[2] ASM Handbook Volume 3: Alloy Phase Diagrams. ASM International, 2016.

[3] C.N. Hsiao, C.S. Chiou, J.R. Yang, Aging reactions in a 17-4 PH stainless steel, Materials Chemistry and Physics **74**, 134-142 (2008).

[4] P. Wanjara, M. Jahazi, Characterization of Electron Beam Welded 17-4 PH Stainless Steel, Canadian Metallurgical Quarterly **47**, 413-435 (2008).

[5] Milad Bahrami Balajaddeh, Homam Naffakh-Moosavy, Pulsed Nd:YAG laser welding of 17-4 PH stainless steel: Microstructure, mechanical properties, and weldability investigation, Optics & Laser Technology **119**, 1-12 (2019).

[6] Yongwei Sun, Yuping Zhong, Lingshui Wang, The interaction between ε-copper and dislocation in a high copper 17-4PH steel, Materials Science and Engineering A **756**, 319-327 (2019).

[7] Guma Yeli, Maria A. Auger, Keith Wilford, Sequential nucleation of phases in a 17-4PH steel, Microstructural characterisation and mechanical properties. Acta Materialia **125**, 38- 49 (2017).

[8] M. Murayama, K. Hono, Y. Katayama, Microstructural evolution in a 17-4 PH stainless steel after aging at 400ºC, Metallurgical and Materials Transactions A **30**, 345-353 (1999).

[9] Zemin Wang, Hui Li, Qin Shen, Nano-precipitates evolution and their effects on mechanical properties of 17-4 precipitation-hardening stainless steel, Acta Materialia **156**, 158-171 (2018).

[10] High -resolution elektron mikroskopy sheet of the structure of Cu particles in α-Fe Philosophical magazine **701**, 24 (1994).

[11] Tao Zhou, R. Prasath Babu, Joakim Odqvist, Hao Yu, Peter Hedström, Quantitative electron microscopy and physically based modelling of Cu precipitation in precipitation-hardening martensitic stainless steel 15-5 PH, Materials & Design **143**, 141-149 (2018).

[12] R. Monzen, M.L. Jenkins, A.P. Sutton, The bcc-to-9R martensitic transformation of Cu precipitates and the relaxation process of elastic strains in an Fe-Cu alloy, Journal Philosophical Magazine A **80**, 711-723 (2000).

[13] Chen-Yuan Chunga, Yu-Chih Tzeng, Effects of aging treatment on the precipitation behavior of ε-Cu phase and mechanical properties of metal injection molding 17-4PH stainless steel, Materials Letters **237**, 228-231 (2019).

[14] A. Ziewiec, A. Zielińska-Lipiec, E. Tasak, Archives of Metallurgy and Materials **59** (3), 965-970 (2014).

[15] K. Bhaduri, T.P.S. Gill, G. Srinivasan, S. Sujith, Science and Technology of Welding and Joining **4** (5), 295-301 (1999).

[16] A. Ziewiec, J. Czech, E. Tasak, Archives of Metallurgy and Materials **57** (4), 1055-1060 (2012).

[17] J. Ma, M.A. Mehdi, L. Wei R. Pillai, B. Kumar, U. Vasudevan, R. Kovacevic, Optics & laser Technology **82**, 38-52 (2016).

[18] A. Nalborczyk-Kazanecka, G. Mrowka-Nowotnik, The Effect of the Parameters of Robotic TIG Welding on the Microstructure of 17-4PH Stainless Steel Welded Joint, Arch. Metall. Mater. **68**, 1, 339-344 (2023).

[19] M. St. Weglowski, S. Błacha, A. Phillips, Electron beam welding – Techniques and trends – Review, Vacuum **130**, 72-92 (2016).

[20] H. Schultz, Electron Beam Welding, Abington Publishing, Cambridge, 1993.